Fatigue Model to Assess Pavement Damage

SHEKHAR GOVIND AND C. MICHAEL WALTON

This paper attempts to derive a general model for fatigue failure. Initially, the problem studied is the relation between the displacement response of a pavement system and the stresses generated by the dynamic application of a load. This is carried out through an analytical model using the theory of wave propagation in an elastic medium. The ultimate objective is forecasting fatigue damage to pavement systems caused by the passage of large trucks. In this regard, a theory is developed to relate fatigue damage to applied stresses. The fatigue model is calibrated by pavement performance data obtained from the AASHO Road Test. Equivalent fatigue damage is computed on a linear damage scale for different axle weights.

In recent years, the number of large combination trucks on the nation's highways has increased dramatically. Many of these trucks have higher axle loads and different axle configurations. This has resulted in increased pavement damage and imprecise forecasts of pavement wear. The end results of the exercise presented in this paper provide a means of forecasting fatigue damage to pavement caused by varied axle configurations and axle weights. Even though the methodology in this case has been applied to predict damage to pavements, the technique developed here is more general and could be applied to any instance where fatigue failure is being studied.

In general, the issue is one of a technique for estimating fatigue damage. In particular, the problem is to determine equivalent axle loads for different axle configurations and axle weights. Starting with the narrower of the two problems, it is known that pavement damage increases nonlinearly with axle weight. Doubling the axle weight would not just double the pavement damage, it would actually raise it by an order of magnitude. The AASHO equivalent single-axle load (ESAL) values were computed on the basis of test data provided by axle loads in the range of 10 to 30 kips. Therefore, extrapolating axle loads beyond 30 kips to forecast pavement wear would be a risky exercise. Further, there is no means of unlinking the damage caused by a steering axle from the damage caused by the load axle of the truck. The methodology developed in this study allows any axle load to be simulated and computes the damage caused by that load with respect to the damage caused by any other axle load.

A similar situation exists in forecasting pavement damage as a function of axle configuration. The AASHO damage equation implicitly recognizes that axles placed in close proximity cause less damage when compared to the same axles placed far apart. For example, the damage caused by a 36-kip tandem axle is approximately 30 percent less than the damage caused by two passes of an 18-kip single axle. However, according to the AASHO formulation, all tandem-axle configurations are treated similarly. It does not matter whether the axles are 2, 4, or 6 ft apart. According to the AASHO equation, all three configurations (with identical axle loads) are calculated to cause the same amount of damage. The fatigue damage model presented here provides for a technique to make a logical distinction among trucks having different axle configurations.

Department of Civil Engineering, University of Texas at Austin, E. Cockrell Jr. Hall, 4.200, Austin, Tex. 78712.

BACKGROUND

A number of experiments have been conducted relating to the effects of dynamic loads on pavements. The stated objective of most of these studies is to determine the effects of dynamic wheel loads on pavement systems. The eventual objective is, ostensibly, to relate dynamic wheel loads to pavement damage, thus advancing pavement design standards or accurately predicting the life of pavement systems for different magnitudes of axle loads. In other words, the entire problem is being viewed at two levels. The first level concerns the accurate estimation of dynamic loads. The second level deals with mapping the dynamic loads by means of transforms, either to produce design criteria or to predict life. The results from studies falling in the first level may indicate that the dynamic response of the system is governed by several factors (vehicle type, all aspects of the vehicle suspension, the speed of the vehicle, the surface profile and pavement composition, and axle loads).

Sweatman (*1*) studied different suspension systems and found that torsion-bar suspensions with hydraulic shock absorbers worked best in reducing dynamic loads. Apart from the study cited here, Lee et al. (*2*) conducted numerous investigations on the different aspects of weigh-in-motion (WIM), for example, the effects of surface profiles on WIM data. In these cases, only the dynamic load at a specific time, $t = t_0$, was obtained, because currently, WIM devices cannot provide the entire spectrum of the load across time. Researchers in other countries have provided a more complete picture of this spectrum (*3*). A method to obtain specific frequency ranges associated with different suspension systems and vehicles was also established by Gillespie et al. (*4*). As noted in this study, almost all of the measured vibrations for a truck fell between frequency values of 0 and 20 Hz.

Sousa et al. (*5*) attempted to determine how the stress field would differ under a moving load, when compared to a static load. Cole and Huth (*6*) also previously examined special cases of this problem; namely, a line load with a constant velocity, versus a static line load. Recent efforts have been

directed at providing a dynamic interpretation of dynaflect measurements. Shao (*7*) studied surface waves (Rayleigh waves) generated by the impact of the falling weight to determine material properties. Sebaaly et al. (*8*) used a multi-degree of freedom elasto-dynamic analysis based on fundamental material properties (e.g., Young's modulus and mass density) to correlate the impact with the measured displacements.

Such techniques are a result of recent advancements in the arena of nondestructive pavement testing by considering wave propagation. Typical examples of this type of research are provided by Shao (*7*) and Douglas and Eller (*9*), who use spectral analysis of surface waves for their dynamic interpretations. The problem, however, remains in the accurate determination of the elastic properties of the different layers present in the pavement system.

PAVEMENT DAMAGE AND AASHO DATA

Several methods are available to classify the state of pavements. These range from a visual inspection and scoring system to making precise measurements on the surface of the pavement to determine the slope variance, rut depth, and other variables. In most cases, each methodology has been constructed for its own specialized information-processing purpose.

Currently, the relative damage caused to pavement by different axle weights is determined by data derived from AASHO Road Tests conducted three decades ago. The empirical formulation is such that all damage estimates are scaled relative to the damage caused by one pass of an 18,000-lb single axle. For example, the damage caused by the passage of one 26,000-lb single axle is calculated to be equivalent to the damage caused by 4.3 passes of an 18,000-lb single axle—or one 44,000-lb tandem axle is calculated to be equivalent to 3.0 passes of an 18,000-lb single axle. In this manner, all damages are scaled on the basis of an ESAL number (*10*).

There could be a number of different ways of looking at the AASHO Road Test data. Both the section on the inner lane and its adjacent section on the outer lane were designed and built together in the same manner. It is, therefore, safe to assume that two sections that are adjacent to each other in the inner and outer lanes, start out with the same value for their present serviceability index (psi). This allows the direct comparison of the number of load applications it took for either lane to get from its original (unknown) psi value to a value of 3.5 psi, for example.

Table 1 is an example of the AASHO Road Test data configured for three sets of ratios of the relative life of identical adjacent flexible pavement sections for Loop Number 6. The only assumed initial difference between adjacent sections in the inner and outer lanes is the applied load. The first and the second columns list the section numbers in Lane 1 and Lane 2, respectively. The third column is the ratio of the number of load applications required in Lane 2 to change the psi value from 3.5 to 3.0 and the number of load applications required in Lane 1 to change the psi value from 3.5 to 3.0. The fourth column is the fraction obtained from the number of load applications on Lane 2 required to change the initial psi value to a psi value of 3.5, divided by the number of load applications on Lane 1 required to change the initial psi value to 3.5. Similarly, the fifth and last column is the fraction obtained from the number of load applications on Lane 2 divided by the number of load applications on Lane 1 for corresponding changes from the initial psi value to 3.0. Data from all the AASHO Road Test flexible pavement loops were similarly coded for this analysis.

TABLE 1 AASHO ROAD TEST DATA FOR FLEXIBLE PAVEMENT SECTIONS IN LOOP 6

Lane 1 Section	Lane 2 Section	L_2/L_1 3.0 to 3.5	L_2/L_1 3.5	L_2/L_1 3.0
307	308	0.2	0.9	0.4
309	310	0.4	1.6	1.1
253	254	0.5	0.7	0.6
329	330	0.6	2.0	1.6
311	312	0.8	3.2	2.0
327	328	0.8	0.4	0.5
271	272	0.8	0.8	0.8
297	298	0.9	1.5	1.3
331	332	0.9	1.2	1.0
303	304	1.1	2.7	2.0
269	270	1.3	3.2	1.7
261	262	1.4	1.4	1.4
321	322	1.4	3.0	2.1
267	268	1.5	1.1	1.2
315	316	1.7	0.9	1.3
323	324	1.8	1.1	1.2
319	320	2.0	2.2	2.2
259	260	2.0	1.0	1.3
313	314	2.3	1.6	2.0
335	336	2.3	0.5	1.1
255	256	2.7	1.0	2.0
325	326	5.0	0.9	1.1
299	300	5.5	1.4	2.7
305	306	6.1	1.4	2.8
317	318	9.2	2.4	4.2
263	264	9.4	1.3	3.3
257	258	18.4	1.1	5.2
Mean		3.00	1.5	1.79
Std. Dev.		3.97	0.79	1.1

SIMULATION MODEL

A brief discussion of the model used to simulate the stress fields generated within the pavement systems of the AASHO experiment follows. A detailed review of these procedures can be found in Govind (*11*). Values of all pertinent variables used in the program correspond to the values of these variables recorded during the AASHO experiment.

Consider an isolated elastic homogeneous layer. Displacements at the top of the layer and the bottom of the layer can be represented by a function of time, $d(t)$. For horizontal displacements (in the plane of the layer), this function could be expanded as a double Fourier series (i.e., a Fourier transform) in Cartesian coordinates. In cylindrical coordinates, the variation in the radial direction would be given by a modified Bessel function of integer order and in the circumferential direction by a Fourier series.

Each term of the series for the displacements maps onto a particular wave number. Further, every term in the infinite series for displacements at the top layer corresponds to a similar term in the series for displacements at the bottom layer. Now, it is possible to determine a closed-form analytical solution and develop a transfer function that relates the top displacements to the bottom ones. A similar procedure can be adopted to obtain the transfer function for stresses as well.

Thompson (*12*) proposed such a model for the propagation of waves in an elastic medium 37 years ago, and it has remained the basis for a majority of the studies conducted since then in this area. Haskell's (*13*) work is also recognized as one of the earlier efforts in this formulation. An alternative to this method has recently been discussed by Kausel and Roesset (*14*), when they applied classical structural analysis concepts to Thompson's techniques and constructed a stiffness matrix for each layer. Their study details how a dynamic stiffness matrix can be obtained by mapping the displacements at the top of a layer to the stresses at the top of the layer (instead of comparing them with the displacements at the bottom of the layer).

By compiling the stiffness matrices for each layer and assembling them, one can obtain the stiffness matrix for the entire pavement structure. This essentially provides a transfer function that relates displacements to stresses at each layer. Because displacements and stress involve Bessel's functions and trigonometric terms, the transfer functions comprising the stiffness matrix will be transcendental functions as well. For each term of the series decomposition (for a particular wave number), a result could be obtained. Finally, the results for each term in the series would have to be combined by numerical integration to obtain a solution for a given load distribution. Such procedures have been implemented both for Cartesian coordinates and cylindrical coordinates.

According to the theoretical formulation, the variation of stress and displacement with depth is described by transcendental functions. If the depth of the layer was small, the variations being studied could be approximated between the top and the bottom of the layer by a straight line—this would represent a linear approximation. Higher order polynomial expansions could also be used here to advantage. In any case, if the layers are thin enough, linear approximations have been found to be extremely efficient in terms of both accuracy and time.

For the case of a half-space soil profile with a rigid bedrock, Waas (*15*) and Kausel (*16*) suggested a procedure to determine the wave numbers and the mode shapes (corresponding to the eigen values and the eigen vectors, respectively) of the propagating waves for a fixed frequency. By transforming these mode shapes, Kausel was also able to obtain explicit solutions for the displacements caused by dynamic loads. As remarked earlier, his formulation is efficient computationally but requires many layers to model deep soil profiles.

Figures 1 through 4 show a typical stress and displacement field generated in the pavement system by the simulation model as a result of the passage of a 3S2 tractor-semitrailer. The observed stress and displacement are similar in nature to the pore pressure curve actually measured under a pavement during the passage of a truck (*17*).

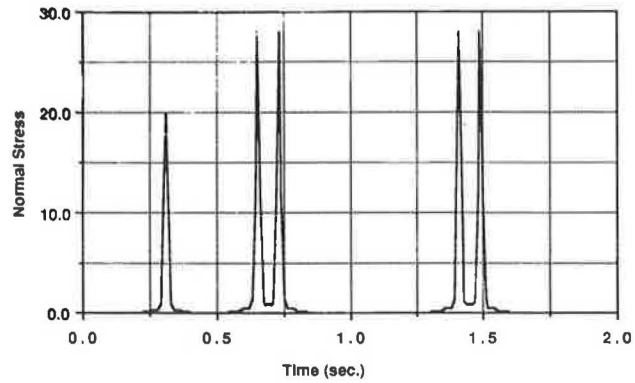

FIGURE 1 Normal stress profile 1 ft below the pavement surface for a 3S2 truck.

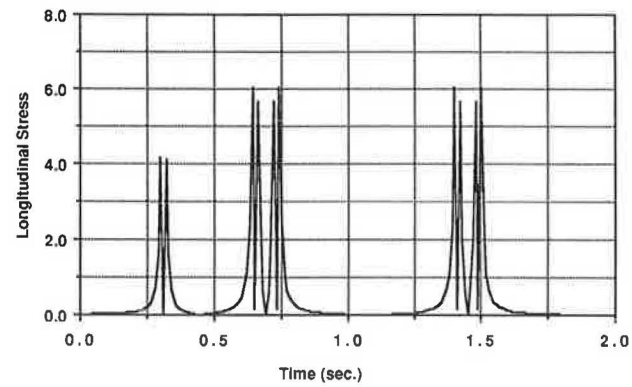

FIGURE 2 Longitudinal stress profile 1 ft below the pavement surface for a 3S2 truck.

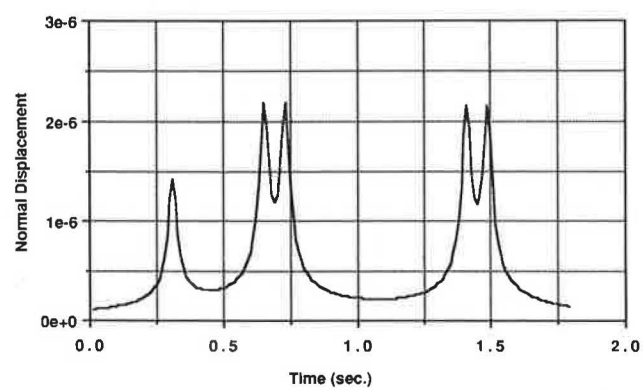

FIGURE 3 Normal displacement 1 ft below the pavement surface for a 3S2 truck.

DESCRIPTION OF MECHANISTIC MODEL

For this study, a finite-element program was implemented to perform stress analysis. The simulation depends on considering steady-state harmonic forces and displacements at a given frequency. These are transmitted through an elastic isotropic medium as compression and shear waves, as well as surface waves. This can be said to be the primary difference between this model and other multi-layered elastic systems.

For a harmonic excitation (caused, say, by a rotating vibrating tire), the solutions at the frequency should correspond directly to the desired displacements. For a transient load, the time history of the force spectrum has to be decomposed into different components using Fourier transforms. Results obtained for each term of the series are then combined and an inverse Fourier transformation is applied to obtain the variation of the displacements over time. Once the displacements and stresses are known at time $t = t_0$, the process is repeated for a new loading position that would correspond to

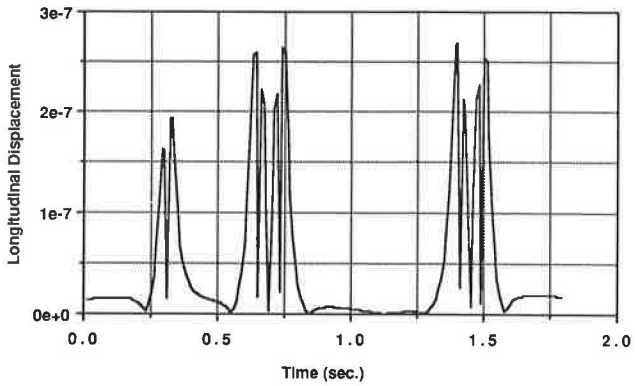

FIGURE 4 Longitudinal displacement 1 ft below the pavement surface for a 3S2 truck.

the driven movement of a vehicle. A time history of stresses can be built in this manner for any location in the pavement system.

Program Review

Six loading schemes are represented in the current program: vertical point load, horizontal point load, vertical disc load, in-plane vertical line load, in-plane horizontal line load, and anti-plane line load. These schemes should be sufficient for our purpose of modeling the vehicle-pavement interaction. The program was tested for different static loads and the result has been found to agree with results obtained through Bousenesque solution and classical elastic theory. Because of the program's large memory requirements, it can be executed on only mainframe computers with one or more gigabytes of memory. The typical execution time on the CRAY-XMP is about 1,000 cpu sec for a 5-axle vehicle driven over 100 ft with 40 discrete frequencies sampled every 0.1 sec.

Input Variables

Input data can be thought of in three groups. The first group deals with the pavement profile. The second group is the frequency ranges to be studied. Finally, the third group of data concerns attributes of the vehicle. A line-by-line discussion of input variables is provided below.

NLAY	Stores the total number of layers in the pavement system. It should include all layers in the pavement, base, subbase, and any geological deposits beneath.
ROCK	This defines the presence of rock or half-space profiles beneath the pavement system. The difference in the behavior of the two profiles would be in their wave-reflection characteristics.
THIK	Defines the thickness of each layer identified in NLAY.
RRO	Contains the value of the mass density of the material in each layer.
VS	Stores the velocity of the shear wave in each layer material.
ANU	Poisson's ratio for the layer material.
DAMP	The damping coefficient that provides the amount of internal damping of each material layer.
NSFR	Number of set of frequencies in the range to be studied.
NFR	Number of frequencies.
OFR	Starting frequency.
DFR	Increment in frequency.
ID	Layer interface where stress and displacement will be computed.
NAXL	Number of axles.
PL	Load on each axle.
X	Spacing between axles.
TRW	Wheel path width.
VEL	Truck velocity.
DX	Incremental movement of load.
LOADT	Load type. Choice of vertical and horizontal point load, disk load, ring load and line load, torsion ring and disk load, and rocking ring and disk load.

Output Variables

There are five output variables. Normal displacements and longitudinal displacements are computed along with normal stresses and longitudinal stresses. These are output along with the time at which these dynamic stresses are recorded. By reducing the input variable, ΔX, it is possible to get as thin a slice of time as is desired. It should be emphasized that apart from the time variable, no units are attached to either the displacement numbers or the stress numbers. The numbers that represent stress and displacement are merely transfer functions that have not been scaled to any particular units and should be used primarily for comparison among themselves.

One limitation of the program is its inability to calculate stresses at the surface of the pavement. This is due to the existence of singularities as point loads are converted to stresses. In computing for different frequencies, a frequency of zero will also produce a singularity.

DAMAGE TRANSFORM

For the purposes of this study, damage transforms are defined as any system of mapping from a load (or stress) domain to a linear damage domain. This concept will be used to transform the simulated stress field of the AASHO experiment to a damage scale, and the results will be compared with the ESAL values established by AASHO to quantify pavement damage as a function of axle loads.

With respect to fatigue, it is not only the magnitude of the force that determines the extent of fatigue damage but also the rate at which it is applied and withdrawn. For cyclic loadings, this is equivalent to assuming that damage would be a function of both the amplitude and the frequency of the load pattern. In other words, it is not just the magnitude of the applied force, stress, or energy that matters in determining the extent of fatigue damage; what also matters is the rate at which it is applied. Therefore, the rate of change of force, stress, or energy might correspond better to our concepts of damage.

A technique of analysis based on similitude study is a prac-

tical approach to addressing this complex engineering problem. In the classical sense, the similitude technique (also referred to as dimensional analysis) consists of a study of three stages. In the first stage, the predominant variables of the problem are recognized for grouping into meaningful dimensionless groups. The second stage in the study consists of setting the criteria for similitude by deciding the relative importance of the dimensionless groups of the variables of the problem. The third stage is the actual execution of the similarity criteria in making a mechanistic model, deciding the kinematic conditions, testing the process, and predicting the behavior of the prototype in view of the dynamic parameters involved.

An attempt is now made to construct a damage model, using dimensional analysis. As discussed earlier, the rate of change of energy (which is power) may be identified as one effective parameter to represent damage. Using the notation L equals the length dimension, T equals the time dimension, and M equals the mass dimension, the following dimensional representations can be stated.

$$\text{Power} = \frac{ML^2}{T^3} \tag{1}$$

A factor not included in our damage discussions so far concerns the size of the specimen being tested for damage. A larger specimen would more likely have a higher capacity to absorb and dissipate the energy it receives as opposed to a smaller specimen with the same material properties. It would seem reasonable that the rate of change of applied energy, or power, should be normalized by the volume of the specimen to account for the size factor. That leads to considering the power expended per unit volume for similitude analysis with damage.

$$\text{Power per unit volume} = \frac{M}{LT^3} \tag{2}$$

Returning briefly to the results obtainable from the dynamic simulation model, it can be stated that the stress and displacement histories of a pavement system can be constructed not only across time at a particular point in space, but also for a particular time at a number of points. In other words, stresses and displacement can be plotted either against time for a constant distance, or they can be plotted against distance at a given value of time. This directly provides us with the following functions.

$$\text{Stress} = f(\text{distance})_{\text{constant time}} = f(\text{time})_{\text{constant distance}}$$

$$\text{Displacement} = f(\text{distance})_{\text{constant time}} = f(\text{time})_{\text{constant distance}}$$

The advantage of representing these variables in their different functional forms is that the exact differential with respect to both time and distance can now be evaluated. For example, consider stress as a function of time. Using the notation ∂ to denote the process of partial differentiation, σ for stress, t for time, and x for distance, the stress function becomes

$$\left[\frac{\partial\sigma(t,x)}{\partial t}\right]_{x=\text{const.}} = \frac{\delta\sigma}{\delta t} \tag{3}$$

The left-hand side of the equation can be evaluated by using the results of the simulation model provided that ∂t, the time increment used, is of a small magnitude. The function could then be represented as

$$\left[\frac{\partial\sigma(t,x)}{\partial t}\right] = \frac{d\sigma}{dt} \tag{4}$$

Examining Equations 2 and 4, it can be seen that they both have the same dimensional form (i.e., power per unit volume and the time rate of change of stress are dimensionally identical).

$$\frac{d\sigma}{dt} = \frac{M}{LT^3} \tag{5}$$

This provides a basis for considering the rate of change of stress (which is dimensionally equivalent to power per unit volume) as one of the parameters used to derive a damage function. This damage function could also be represented as a stress-ratio dimensionless number by comparing the damage caused by one event with the damage caused by another event.

To relate the function to specific events of stress application over time, some form of average or sum over the time period of the event would have to be evaluated. Absolute values for the exact differential would have to be used in the averaging process because a negative rate of change of stress would tend to cancel out the positive rate of change of stress in a symmetrical stress-time curve with the axis of symmetry parallel to the stress axis. This would be further justified if one kept in mind that it is the cumulative effect of all subevents within an event that should be accounted for, and averaging is the simplest of the many techniques to accomplish it. If the differential is summed over time, some form of normalization with respect to time should also be considered. An event that allowed more than one stress peak to occur could be divided into subsets of smaller events, each containing only one stress peak (i.e., one stress cycle per event subset). The effect of the event in its totality will be represented by a cumulative sum of the effects of the event in each subset.

In accordance with the above discussions, the formulation of the methodology of one damage transform follows. Consider a loading event, R, that generates a stress field, $\sigma(t)$. The function defining $\sigma(t)$ is such that m changes occur in the sign of the slope of the stress curve. The time, t, at each successive change of the slope from negative to positive is denoted by $(t_1 \ldots t_m)$. The peak P_1 starts at time $t = t_0$ and ends at time $t = t_1$; the peak P_2 starts at time $t = t_1$ and ends at time $t = t_2$ and so on. For the event R, the cumulative effect of the m different subevents could be represented by an nth power for each peak.

$$\left(\frac{1}{t_1 - t_0}\int_{t_0}^{t_1}\left|\frac{\delta\sigma}{dt}\right| dt\right)^n + \left(\frac{1}{t_2 - t_1}\int_{t_1}^{t_2}\left|\frac{\delta\sigma}{dt}\right| dt\right)^n + \ldots \tag{6}$$

For the final result to be sensitive to all individual subevents, the sum for each peak must be raised to the power n

before being added. That assumes the transform is a power law function.

Once such summations are obtained for separate events, it should now be possible to obtain a dimensionless rate of change of stress (or power per unit volume) ratio that would compare the effects of the different events. Let us denote for the event R comprising m separate subevents D_i, each D comprises a single stress peak.

$$\sum_{i=1}^{m} D_i^n = \sum_{i=1}^{m} \left(\frac{1}{t_{i-1} - t_i} \int_{t_{i-1}}^{t_i} \left| \frac{\delta\sigma}{dt} \right| dt \right)^n \tag{7}$$

If now it was decided to compare the effect of the damage caused by a single-peak event, R_a (having a dimensionless number, D_a, denoting damage by the only stress peak) as a fraction of the damage caused by a single-peak event R_b (having a dimensionless number, D_b, denoting damage by the only stress peak), the ratio of the two damages could be computed by Equation 8. In this equation, L denotes the life of the specimen.

$$\left(\frac{D_a}{D_b}\right)^n = \left(\frac{L_b}{L_a}\right) \tag{8}$$

Here, L_a and L_b would correspond to the effective number of loading/unloading cycles to failure of the two specimens undergoing the events a and b (i.e., they are the variables denoting life).

The damage transform seen in Equation 8 is conceptually similar to ideas proposed by Palmgren (*18*) in his treatise on the phenomenon of fatigue failure in ball and roller bearings. The main difference between the two procedures is that Palmgren used force as his choice of variable from which to derive a dimensionless ratio. His number corresponds to a dimensionless force ratio and depicts the ratio of the life, L_1, as determined by force, F_1, with respect to the life, L_2, as determined by force, F_2. Palmgren found that, for his data, the best regression fit was obtained for n equals 3.

$$\left(\frac{F_1}{F_2}\right)^n = \left(\frac{L_2}{L_1}\right) \tag{9}$$

The damage numbers, D_i and D_k, can be thought of in terms similar to that proposed by Palmgren. The difference would be that instead of force ratios, power per unit volume ratios are used. The value of n would be quite different in Equations 8 and 9, being dependent on the interactions of a host of variables that are completely different for ball bearings and pavements. One can now establish the relation presented in Equation 8. The damage number derived from this representation may be more accurate in predicting actual damage than the ESAL numbers because of reasons outlined earlier. This methodology may be applied to determine the relative damage caused by any event with respect to the damage caused by another event.

It should be pointed out that other similar dimensionless numbers can also be derived here using not just stress, but a host of other functions as well. Not all these dimensionless damage numbers may eventually be independent of each other as per Buckingham's π theorem, which provides that a set of n physical quantities with r base dimensions may always be arranged to form an infinite number of dimensionless groups, of which only $(n - r)$ dimensionless parameters are independent. Therefore, if two or more variables from elasticity are finally transformed onto a damage scale, all would not be expected to be independent.

DISCUSSION OF RESULTS

The results presented and discussed here deal with the calibration of the proposed fatigue model. Initially, a regression model was used to determine the bounds of the value of n in the equations

$$D = \int_{t_0}^{t_1} \frac{1}{t_1 - t_0} \left| \frac{\delta\sigma}{dt} \right| dt \tag{10}$$

and

$$\left(\frac{D_a}{D_b}\right)^n = \left(\frac{L_b}{L_a}\right) \tag{11}$$

where D_a and D_b are the damage transforms for the events a and b, and L_a and L_b are the lives of the specimens for the events a and b, respectively.

The data used to calibrate the model were obtained from the AASHO Road Test data set and comprise the data for flexible pavements (Table 1 is an example of the data from Loop Number 6). The traffic on each lane was simulated to obtain the damage transforms, and the value of n was found so as to equate the life ratios as a power of the ratios of the damage transform.

A regression was performed on these data with the intent of finding the range of the value that the variable n could take and not just with the idea of fixing the best fit on the data with a particular value of n. Once a range had been determined for the variable, it would be easy to check how the equation behaved for different values of n within the bounds. In effect, a sensitivity analysis of the equation could now be performed and the results compared to the AASHTO ESAL values. Figure 5 shows the plot of the residual sum of squares

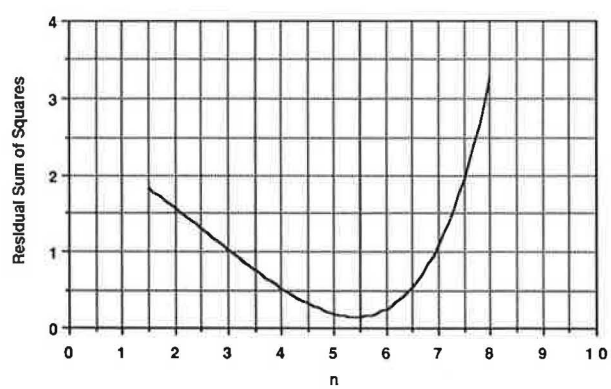

FIGURE 5 Residual sum of squares plotted against *n* for Equations 10 and 11, using AASHO Road Test data for flexible pavements.

for Equation 11 and life ratios of initial to 3.5 psi plotted with respect to the values of n. From Figure 5, it can be seen that the value of the sum of squares is below 1 for n values between 3.0 and 7.0, with a smaller rate of change of slope observed toward the value of 3.0 than toward 7.0, where a rapid rate of change of slope can be seen. This implies that the actual value of n may be more biased toward 3.0 than toward 7.0 or higher. In any event, the range $3 \leq n \leq 7$ should clearly provide us with a value of n that would serve as a good model for the AASHO data.

Tables 2 through 7 show how the ESAL values for different axle loads are computed according to Equations 10 and 11 with respect to a single 18-kip axle load for different values of n. The denominator, D_b, in the damage ratio of Equation 11 corresponds to the stress peak for a standard 18-kip single axle. Therefore, these tables are identical to computing 18-kip ESAL factors. Table 8 lists the ESAL values used by AASHO for a flexible pavement at a psi of 3.0. On inspection, it can be seen that the ESAL values for n in the range computed here are similar to the range of ESAL values provided by AASHO. For example, when n equals 4.6 (Table 2), the equivalent damage for different axle loads predicted by the model corresponds closely to the ESAL factors established by AASHO for a pavement at a psi of 3.0 and a structural number of 1 (Table 8).

CONCLUSIONS

By comparing the AASHO ESAL values for different psi levels and the ESAL values computed by means of the damage model (Tables 2 through 8), it is apparent that both equivalency factors belong to the same family of damage curves. The techniques used in this study can be easily applied to axle load ranges that were not covered by the AASHO Road Test data and precise ESAL values obtained for those ranges. This methodology has also been applied to determine damage numbers resulting from the effects of axle spacing in tandem axles (*19*). This is another area where AASHO equivalents are not precise.

TABLE 2 SENSITIVITY ANALYSIS OF ESAL WITH RESPECT TO n IN EQUATION 11: n-VALUES 4.70–4.50

Load (kips)	n Values				
	4.70	4.65	4.60	4.55	4.50
2	0.00	0.00	0.00	0.00	0.00
4	0.00	0.00	0.00	0.00	0.00
6	0.01	0.01	0.01	0.01	0.01
8	0.02	0.02	0.02	0.03	0.03
10	0.06	0.07	0.07	0.07	0.07
12	0.15	0.15	0.15	0.16	0.16
14	0.31	0.31	0.32	0.32	0.33
16	0.58	0.58	0.58	0.59	0.59
18	1.00	1.00	1.00	1.00	1.00
20	1.64	1.64	1.63	1.62	1.61
22	2.56	2.54	2.51	2.49	2.46
24	3.89	3.83	3.78	3.72	3.67
26	5.64	5.54	5.44	5.34	5.24
28	8.04	7.86	7.69	7.52	7.35
30	10.85	10.58	10.31	10.06	9.80
32	14.90	14.48	14.07	13.67	13.29
34	20.06	19.43	18.82	18.23	17.66
36	26.63	25.71	24.83	23.98	23.16
38	33.55	32.32	31.13	29.99	28.89
40	43.27	41.57	39.94	38.37	36.86
42	54.12	51.87	49.71	47.65	45.66
44	65.87	63.00	60.26	57.63	55.12
46	82.41	78.63	75.02	71.58	68.30
48	100.99	96.16	91.55	87.16	82.99
50	120.62	114.62	108.93	103.51	98.37

TABLE 3 SENSITIVITY ANALYSIS OF ESAL WITH RESPECT TO n IN EQUATION 11: n-VALUES 4.45–4.25

Load (kips)	n Values				
	4.45	4.40	4.35	4.30	4.25
2	0.00	0.00	0.00	0.00	0.00
4	0.00	0.00	0.00	0.00	0.00
6	0.01	0.01	0.01	0.01	0.01
8	0.03	0.03	0.03	0.03	0.03
10	0.07	0.08	0.08	0.08	0.08
12	0.16	0.17	0.17	0.17	0.18
14	0.33	0.33	0.34	0.34	0.35
16	0.59	0.60	0.60	0.61	0.61
18	1.00	1.00	1.00	1.00	1.00
20	1.60	1.59	1.58	1.58	1.57
22	2.44	2.41	2.39	2.37	2.34
24	3.61	3.56	3.51	3.46	3.41
26	5.14	5.05	4.96	4.87	4.78
28	7.19	7.04	6.88	6.73	6.58
30	9.56	9.32	9.09	8.86	8.64
32	12.91	12.54	12.19	11.84	11.51
34	17.10	16.57	16.05	15.54	15.06
36	22.36	21.59	20.85	20.14	19.45
38	27.83	26.81	25.83	24.88	23.97
40	35.41	34.02	32.68	31.40	30.17
42	43.77	41.95	40.20	38.53	36.93
44	52.72	50.42	48.23	46.12	44.11
46	65.17	62.18	59.33	56.61	54.02
48	79.01	75.23	71.62	68.19	64.92
50	93.48	88.83	84.41	80.22	76.23

TABLE 4 SENSITIVITY ANALYSIS OF ESAL WITH RESPECT TO n IN EQUATION 11: n-VALUES 4.20–4.00

Load (kips)	n Values				
	4.20	4.15	4.10	4.05	4.00
2	0.00	0.00	0.00	0.00	0.00
4	0.00	0.00	0.00	0.00	0.00
6	0.01	0.01	0.01	0.01	0.01
8	0.03	0.04	0.04	0.04	0.04
10	0.09	0.09	0.09	0.09	0.10
12	0.18	0.19	0.19	0.19	0.20
14	0.35	0.36	0.36	0.37	0.37
16	0.61	0.62	0.62	0.62	0.63
18	1.00	1.00	1.00	1.00	1.00
20	1.56	1.55	1.54	1.53	1.53
22	2.32	2.30	2.27	2.25	2.23
24	3.36	3.31	3.27	3.22	3.17
26	4.69	4.61	4.52	4.44	4.36
28	6.44	6.30	6.16	6.02	5.89
30	8.42	8.21	8.00	7.80	7.61
32	11.18	10.86	10.56	10.26	9.97
34	14.58	14.13	13.68	13.25	12.84
36	18.78	18.13	17.51	16.91	16.33
38	23.09	22.24	21.42	20.64	19.88
40	28.98	27.84	26.75	25.70	24.69
42	35.40	33.92	32.51	31.16	29.87
44	42.19	40.35	38.60	36.91	35.31
46	51.54	49.18	46.92	44.77	42.72
48	61.81	58.85	56.03	53.35	50.79
50	72.44	68.84	65.42	62.17	59.08

TABLE 5 SENSITIVITY ANALYSIS OF ESAL WITH RESPECT TO *n* IN EQUATION 11: *n*-VALUES 3.95–3.75

Load (kips)	n Values				
	3.95	3.90	3.85	3.80	3.75
2	0.00	0.00	0.00	0.00	0.00
4	0.00	0.00	0.00	0.00	0.00
6	0.01	0.01	0.01	0.02	0.02
8	0.04	0.04	0.04	0.05	0.05
10	0.10	0.10	0.10	0.11	0.11
12	0.20	0.21	0.21	0.21	0.22
14	0.37	0.38	0.38	0.39	0.39
16	0.63	0.63	0.64	0.64	0.65
18	1.00	1.00	1.00	1.00	1.00
20	1.52	1.51	1.50	1.49	1.49
22	2.21	2.18	2.16	2.14	2.12
24	3.13	3.08	3.04	3.00	2.95
26	4.28	4.20	4.12	4.05	3.98
28	5.76	5.64	5.51	5.39	5.27
30	7.42	7.23	7.05	6.87	6.70
32	9.68	9.41	9.14	8.88	8.63
34	12.43	12.04	11.66	11.30	10.94
36	15.77	15.23	14.71	14.20	13.72
38	19.15	18.45	17.77	17.12	16.49
40	23.72	22.79	21.89	21.03	20.21
42	28.62	27.43	26.29	25.20	24.15
44	33.77	32.30	30.89	29.54	28.26
46	40.76	38.89	37.11	35.41	33.78
48	48.36	46.04	43.83	41.73	39.74
50	56.14	53.35	50.70	48.18	45.78

TABLE 6 SENSITIVITY ANALYSIS OF ESAL WITH RESPECT TO *n* IN EQUATION 11: *n*-VALUES 3.70–3.50

Load (kips)	n Values				
	3.70	3.65	3.60	3.55	3.50
2	0.00	0.00	0.00	0.00	0.00
4	0.00	0.00	0.00	0.00	0.01
6	0.02	0.02	0.02	0.02	0.02
8	0.05	0.05	0.05	0.06	0.06
10	0.11	0.12	0.12	0.12	0.13
12	0.22	0.23	0.23	0.24	0.24
14	0.40	0.40	0.41	0.41	0.42
16	0.65	0.65	0.66	0.66	0.66
18	1.00	1.00	1.00	1.00	1.00
20	1.48	1.47	1.46	1.46	1.45
22	2.10	2.08	2.06	2.04	2.02
24	2.91	2.87	2.83	2.79	2.75
26	3.90	3.83	3.76	3.69	3.63
28	5.16	5.05	4.93	4.83	4.72
30	6.53	6.37	6.21	6.06	5.90
32	8.39	8.15	7.92	7.70	7.48
34	10.60	10.27	9.94	9.63	9.33
36	13.24	12.79	12.35	11.93	11.52
38	15.89	15.30	14.74	14.20	13.68
40	19.41	18.65	17.92	17.21	16.54
42	23.15	22.19	21.27	20.38	19.53
44	27.02	25.85	24.72	23.64	22.61
46	32.23	30.76	29.35	28.00	26.72
48	37.83	36.02	34.29	32.65	31.09
50	43.51	41.34	39.29	37.34	35.48

TABLE 7 SENSITIVITY ANALYSIS OF ESAL WITH RESPECT TO *n* IN EQUATION 11: *n*-VALUES 3.45–3.30

Load (kips)	n Values			
	3.45	3.40	3.35	3.30
2	0.00	0.00	0.00	0.00
4	0.01	0.01	0.01	0.01
6	0.02	0.02	0.03	0.03
8	0.06	0.06	0.07	0.07
10	0.13	0.14	0.14	0.14
12	0.25	0.25	0.26	0.26
14	0.42	0.43	0.43	0.44
16	0.67	0.67	0.68	0.68
18	1.00	1.00	1.00	1.00
20	1.44	1.43	1.43	1.42
22	2.00	1.98	1.96	1.94
24	2.71	2.67	2.63	2.59
26	3.56	3.50	3.43	3.37
28	4.62	4.52	4.42	4.32
30	5.76	5.61	5.47	5.33
32	7.27	7.06	6.86	6.67
34	9.04	8.75	8.48	8.21
36	11.12	10.74	10.37	10.02
38	13.18	12.70	12.23	11.78
40	15.89	15.26	14.66	14.09
42	18.72	17.94	17.20	16.48
44	21.63	20.69	19.78	18.92
46	25.49	24.32	23.21	22.14
48	29.60	28.18	26.83	25.54
50	33.72	32.04	30.45	28.93

TABLE 8 ESAL FACTORS FOR FLEXIBLE PAVEMENTS AT A PSI OF 3.0 (*10*)

Load (kips)	Pavement Structural Number (SN)					
	1	2	3	4	5	6
2	0.00	0.00	0.00	0.00	0.00	0.00
4	0.00	0.00	0.01	0.00	0.00	0.00
6	0.01	0.03	0.03	0.02	0.01	0.01
8	0.04	0.07	0.08	0.06	0.04	0.03
10	0.08	0.13	0.17	0.13	0.10	0.09
12	0.17	0.23	0.30	0.26	0.21	0.19
14	0.33	0.39	0.47	0.45	0.39	0.36
16	0.59	0.63	0.69	0.69	0.65	0.62
18	1.00	1.00	1.00	1.00	1.00	1.00
20	1.60	1.53	1.41	1.38	1.44	1.51
22	2.47	2.29	1.96	1.83	1.97	2.16
24	3.67	3.33	2.69	2.39	2.60	2.96
26	5.29	4.72	3.65	3.08	3.33	3.91
28	7.43	6.56	4.88	3.93	4.17	5.00
30	10.20	8.90	6.50	5.00	5.10	6.30
32	13.80	12.00	8.40	6.20	6.30	7.70
34	18.20	15.70	10.90	7.80	7.60	9.30
36	23.80	20.40	14.00	9.70	9.10	11.00
38	30.60	26.20	17.70	11.90	11.00	13.00
40	38.80	33.20	22.20	14.60	13.10	15.30
42	48.80	41.60	27.60	17.80	15.50	17.80
44	60.60	51.60	34.00	21.60	18.40	20.60
46	74.70	63.40	41.50	26.10	21.60	23.80
48	91.20	77.30	50.30	31.30	25.40	27.40
50	110.00	94.00	61.00	37.00	30.00	32.00

With respect to the physical significance of n, it could represent the structural strength of the pavement. A lower value of n might imply a strong and well-designed pavement with respect to the load being carried on it, while a higher value of n would be used for pavements that are underdesigned for the load they experience. In this respect, n behaves as an inverse function of the pavement structural number (SN), the index used by AASHO to quantify the quality of pavements. An interesting side note to Equation 11 is that because the ratio of the damage transforms D_a and D_b is being raised to a power n, when D_a is less than D_b the nature of the family of damage curves changes. For this reason, Equation 11 should be used only if D_a is greater than D_b.

In conclusion, it should be stated that the damage model developed and presented here provides an excellent alternative to the AASHO values for 18-kip ESAL. Further, when compared to the AASHO procedure, it also provides a more accurate means of determining the ESAL for tandem axles with nonuniform spacings. It should also be recognized that the methodology is completely general and may be used for studying any fatigue damage-related phenomenon.

REFERENCES

1. P. F. Sweatman. *A Study of Dynamic Wheel Forces in Axle Group Suspensions of Heavy Vehicles*. Special Report No. 27, Road Research Board, June 1983.
2. C. E. Lee, B. Izadmehr, and R. B. Machemehl. *Demonstration of Weigh-In-Motion Systems for Data Collection and Enforcement*. Research Report 557-1F, Center for Transportation Research, University of Texas at Austin, Austin, Tex., Dec. 1985.
3. D. R. Leonard, J. W. Grainger, and R. Eyre. *Loads and Vibrations Caused by Eight Commercial Vehicles with Gross Weight Exceeding 30 Tons*. TRRL Laboratory Report 582, Transport and Road Research Laboratory, Great Britain, 1974.
4. T. D. Gillespie, et al. *Influence of Size and Weight Variables on the Stability and Control Properties of Heavy Trucks*. Report No. UMTRI-83-10/2, University of Michigan, 1983.
5. J. B. Sousa, J. Lysmer, S. S. Chen, and C. L. Monismith. *Response of Asphalt Concrete Pavements to Dynamic Truck Loads*. Institute of Transportation Studies, University of California, Berkeley, March 1987.
6. J. Cole and J. Huth. Stresses Produced in a Half-Plane by Moving Loads. *Journal of Applied Mechanics*, Dec. 1958, p. 433.
7. K-Y. Shao. Dynamic Interpretation of Dynaflect, Falling Weight Deflectometer and Spectral Analysis of Surface Waves Tests on Pavement Systems. Ph.D. dissertation. Department of Civil Engineering, University of Texas at Austin, Austin, Tex., Dec. 1985.
8. B. E. Sebaaly, M. S. Mamlouk, and T. G. Davies. Dynamic Analysis of Falling Weight Deflectometer Data. In *Transportation Research Record 1070*, TRB, National Research Council, Washington, D.C., 1986, pp. 63–68.
9. R. A. Douglas and G. L. Eller. Nondestructive Pavement Testing by Wave Propagation: Advanced Methods of Analysis and Parameter Management. In *Transportation Research Record 1070*, TRB, National Research Council, Washington, D.C., 1986, pp. 53–64.
10. *AASHTO Interim Guide for Design of Pavement Structures*. AASHTO, Washington, D.C., 1985.
11. S. Govind. A Dynamic Analysis of Pavement Systems to Determine a Damage Transform from Stress Fields. Ph.D. dissertation. Department of Civil Engineering, University of Texas at Austin, Austin, Tex., May 1988.
12. W. T. Thompson. Transmission of Elastic Waves through a Stratified Soil Medium. *Journal of Applied Physics*, Vol. 21, Feb. 1950.
13. N. A. Haskel. The Dispersion of Surface Waves on Multilayered Media. BSSA, Vol. 43, No. 1, Feb. 1953.
14. E. Kausel and J. M. Roesset. Stiffness Matrix for Layered Soils. BSSA, Vol. 71, No. 6, Dec. 1981.
15. G. Waas. Linear Two-Dimensional Analysis of Soil Dynamics Problem on Semi-Infinite Layered Media. Ph.D. dissertation. Department of Civil Engineering, University of California, 1972.
16. E. Kausel. *An Explicit Solution for the Green Functions for Dynamic Loads in Layered Media*. Research Report R81-13. Department of Civil Engineering, Massachusetts Institute of Technology, Cambridge, 1981.
17. M. Hyodo, K. Yasahara, and H. Murata. Traffic-Induced Pore Pressure and Deformation of Soft Clay Deposit Beneath Embankment. *Proc., International Symposium on Geotechnical Engineering in Soft Soils*, Mexico City, 1987.
18. A. Palmgren. *Ball and Roller Bearing Engineering*. S. H. Burbank & Co., Inc., Philadelphia, Pa., 1945.
19. S. Govind, D. A. Faria, R. B. Machemehl, and C. M. Walton. *Analysis and Forecast of Truck Traffic Loads and the Relative Damage to Pavement Systems as a Function of Axle Configurations*. Research Report Number 378-1F. Center for Transportation Research, The University of Texas at Austin, Nov. 1987.

Publication of this paper sponsored by Committee on Flexible Pavement Design.